Communication

High efficiency power management and charge boosting strategy for a triboelectric nanogenerator

CrossMark

Xiaoliang Cheng[a], Liming Miao[a], Yu Song[a], Zongming Su[a], Haotian Chen[a,b], Xuexian Chen[a,b], Jinxin Zhang[a], Haixia Zhang[a,*]

[a] National Key Laboratory of Nano/Micro Fabrication Technology, Peking University, 100871 Beijing, China
[b] Academy for Advanced Interdisciplinary Studies, Peking University, Beijing 100871, China

A B S T R A C T

Triboelectric nanogenerator (TENG) has emerging as an important approach for energy harvesting. However, low charging efficiency as well as low power conversion efficiency have restricted its practical application for powering traditional electronics. Here we propose a power management (PM) strategy by extracting maximum energy from TENG and transferring the energy to storage unit employing optimized Inductor-Capacitor (LC) oscillating. PM module using this strategy designed shown universality and high-efficiency for different modes TENG. Over 2600 times improvement in stored energy than standard circuit was achieved, and more than 72% alternating current (AC) to direct current (DC) power transfer efficiency was obtained for different modes TENGs. The regulated and managed output shown the ability as a power source for the continuously working of commercial electronics, such as LED bulbs, calculators and pedometers. Our work provides an effective, universal and practical strategy for efficiently power management of TENG from theoretical derivation and experimental validation, which is promising to serve as a standard PM module for TENG as well as to guide its design.

1. Introduction

The tremendous development in wearable electronics [1], wireless sensor nodes [2] and implantable electronic devices [3] has raised urgent and challenging requirements for developing sustainable and stable power source. Though batteries or capacitors [4–6], as the traditional energy storage unit, are the mostly used power source for these devices, the limited capacity and large volume make them have to be frequently charged or replaced thus becoming more and more unpractical and unfavorable. One of the most promising methods to overcome such difficulties is the employment of energy-harvesting technologies from the ambient environment or human motion for sustainable operation [7,8]. To date, the most commonly adopted mechanisms are electromagnetic induction [9], electrostatic induction [10] and piezoelectric effect [11], while different mechanisms show particular advantages to specific applications. Recently, the emerging energy conversion method, called triboelectric nanogenerator (TENG), is rising as a potential technology, which has the advantages of high output, simple design, and low cost [12–16]. Various mechanical energy sources from water wave [17], wind [18], human motions [19] and even heartbeat [20] have been successfully converted to electric energy by TENG.

However, working as a capacitive-behavior energy harvester, TENG has a high inherent impedance of typically in several Mega ohms' level with high voltage of typically hundreds of volts and low output current (i.e. in ~µA level) [13,21]. These characteristics lead to low energy transfer efficiency for either powering electronics [22] or charging a battery/capacitor directly, since usually they have relatively low impedance. A proper power management strategy is thereby required for TENG towards powering electronics and charging energy storage unit (i.e. battery or capacitor). From the features of output waveform, TENG includes two basic modes that are contact-separation mode (CS mode, including classical contact-separation mode [23] and single-electrode mode [24]) with low-frequency randomly-pulsed waveform and lateral-sliding mode (LS mode, including classical lateral sliding mode [25] and free-standing mode [26]) with uniform triangular waveform [27]. For the LS mode, a transformer with matched frequency has a satisfied performance [28,29] Unfortunately, a huge power loss would occur once the working frequency changes, while the frequency of mechanical energy typically is very low and varies in a very wide range, which makes the transformer even incapable for the LS-mode TENG. As for the CS mode, the randomly-pulsed waveform is much harder to manage [30]. Consequently, there is an urgent requirement for a universal applicable power-management

---

strategy for both modes TENG. Recently, as an alternative method, Niu et al. proposed a power management system for TENG using a matched capacitor as a bridge between TENG and management circuit, which shown good performance for CS-mode TENG [31]. But at least 25% energy loss would produce between energy transfer from TENG to the bridge capacitor, and this capacitor has to be optimized for TENGs with different parameters, making it inefficient and unpractical.

In this work, we aim at solving the mentioned challenge by designing and proposing an efficient, universal and practical power management strategy (PMS) for TENG. To achieve the goal, a two-steps strategy is adopted: (1) Maximizing the output energy of a TENG by using built-up voltage V-total transferred charges Q plot applicable

to both-modes TENG; (2) Maximizing the transferred energy from TENG to energy storage unit by employing the LC oscillating model. Afterwards, a power management module (PMM) was designed and assembled under the guidance of this strategy to manage and regulate the electric outputs from CS-TENG and LS-TENG. Using this module, both huge improvements were achieved for the stored charges and energy in energy storage unit. Meanwhile, more than 70% power conversion efficiencies were obtained for both modes TENG. The regulated and managed direct current (DC) power can provide a continuously power source for driving conventional electronics, such as LED bulbs, calculators, pedometers. Our work proposed a strategy for designing universal and efficient PMM for TENG, which would set
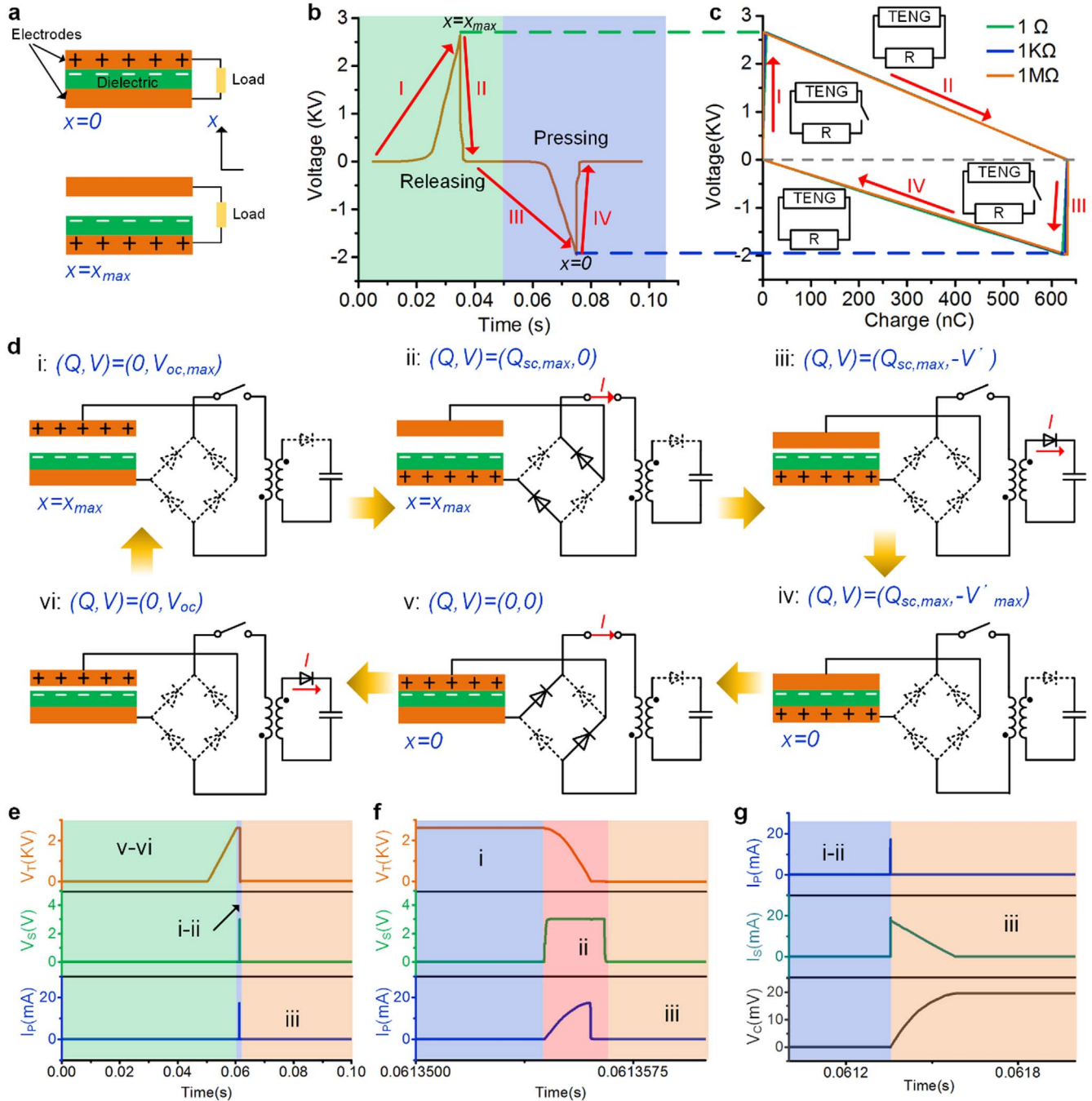

Fig. 1. Operating cycles of PMS for TENG. (**a**) Schematic diagram of the CS-mode TENG with displacement x = 0 and x = x$_{max}$. (**b**) The simulated output voltage of TENG using the PMS by SPICE. The displacement position, the state of applied force and the corresponding state in Fig. 1c were marked, respectively. (**c**) The CMEO with 1 Ω, 10 Ωand 100 MΩ load resistance. The inserts show the corresponding status of the switch in circuits during different steps. (**d**) Operating cycles for scavenging maximum energy from TENG and transferring it to capacitor via LC oscillating. (**e–g**) The simulated results of signals in circuits of (**d**). And the corresponding status of (**d**) was marked.

the foundation for the further applications and industrialization of the TENGs.

2. Results

2.1. Design for maximized energy output of TENG with serial switch

To maximum the output energy of power management system, the output energy of TENG should be maximized first. Based on the relationship among the transferred charges between the electrode Q, the built-up voltage V and the relative displacement x between the triboelectric layer, the governing equations of TENG can be developed. The definitions of the displacement x and the two electrodes for an CS-mode TENG are illustrated in Fig. 1a. According to previous work [31],

both the absolute short-circuit transferred charges $Q_{SC}(x)$ and the absolute open-circuit voltage $V_{OC}(x)$ at $x = 0$ position are set to be 0, and the maxima of $Q_{SC,max}$ and $V_{OC,max}$ are expected to be reached at $x = x_{max}$ simultaneously for all basic-mode TENGs. The output energy per cycle E at a certain period of time T can be derived as [32]:

$$E = \overline{P}T = \int_0^T VIdt = \int_{t=0}^{t=T} VdQ = \oint VdQ \tag{1}$$

Where $\overline{P}$ is the average output power from TENG. Therefore, we can use the *V-Q* plot to calculate the output energy of TENG in a cycle by calculating the encircled area of the closed loop in the *V-Q* curve.

Using the *V-Q* plot, previous studies [32] developing a parallel-switch strategy to obtain the cycles for maximized energy output (CMEO) of TENG. However, the maximized energy can be only
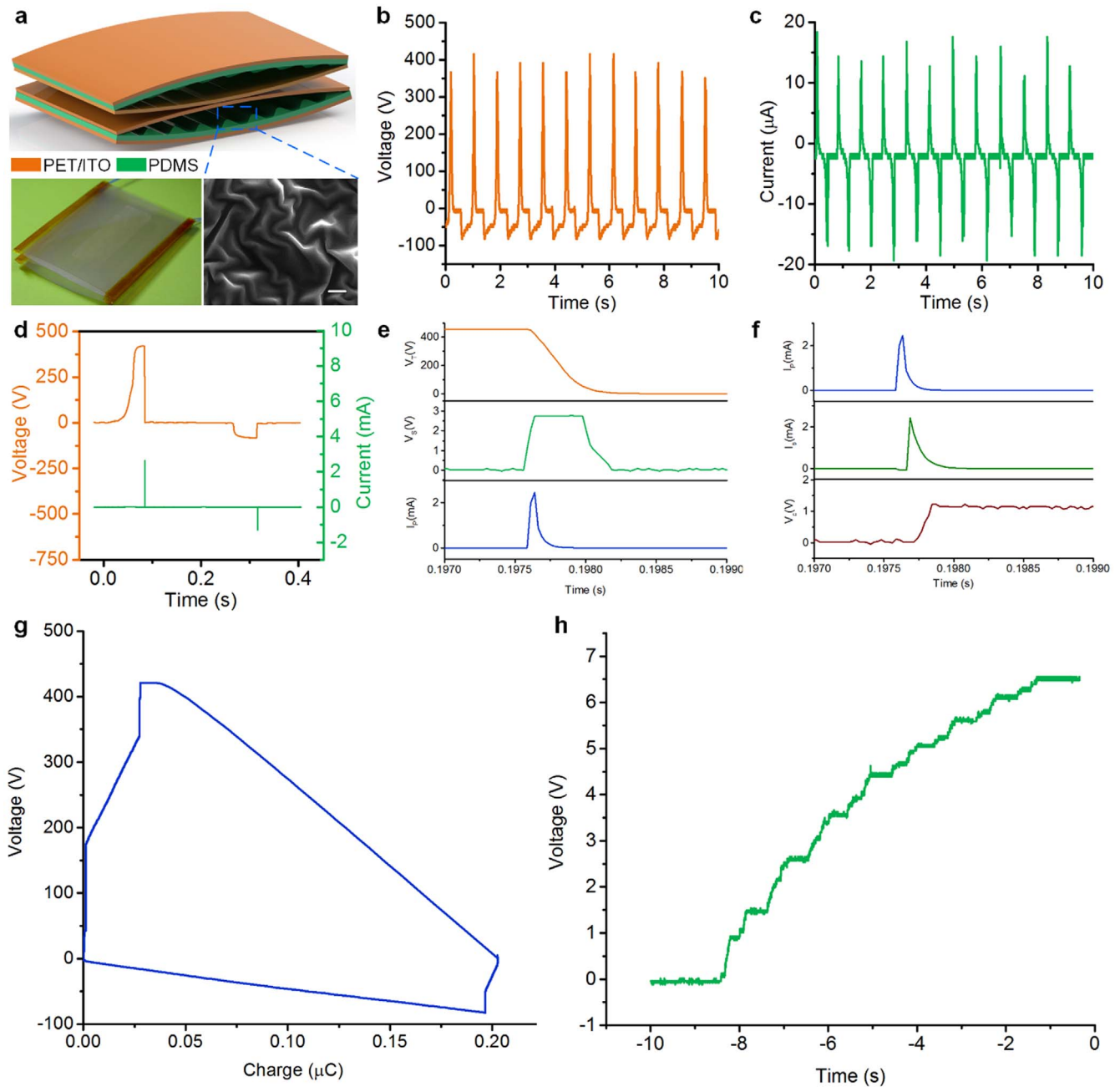

Fig. 2. Experimental results using PMM for CS-mode TENG. (**a**) Schematic diagram of the CS-mode TENG using in this work. The photograph and SEM image of the wrinkle structure were inserted. (**b**–**c**) Waveforms of output voltage and current of the CS-mode TENG. (d) Measured voltage and current curves of CS-mode TENG using PMM. (e) Experimental results of waveform in primary circuit of PMM (V_T, V_S and I_P denote the voltage of TENG, the voltage of switch controlling signal, and current of primary inductor). (f) The curves of currents in coupled inductor and voltage of stored capacitor. (g) V-Q plot of CS-mode TENG using PMM. (h) Charging curve of CS-mode TENG using PMM for a 10 μF capacitor.

achieved at $R = +\infty$, namely the open-circuit condition, which actually further increase the effective impedance of TENG and the difficulty for the design of power management system. To obtain CMEO at a lower resistance, we adopt the serial-switch design, which has been used to for obtaining maximized energy from a TENG [33]. To better understand this design, the output voltage of TENG with 1MΩ and V-Q plots at 1 Ω, 1KΩ and 1MΩ were simulated by finite element method (FEM) and SPICE software as shown in Fig. 1b-c (Corresponding parameters are listed in Supplementary table 1). Noticing that TENG produces $Q_{sc,max}$ at a relative low resistance, if we could obtain the $V_{OC,max}$ at a low resistance, the CMEO could be reached. The operation for serial-switch design works as following: step I, the upper part displaces relatively from $x = 0$ to $x = x_{max}$ at switch off to enable $V^{=}V_{OC,max}$; step II, turn the switch on to enable current flow in outer resistor to make $Q = Q_{SC,max}$ then turn the switch off; step III, the upper part moves relatively from $x = x_{max}$ to $x = 0$ at switch off to enable $V = -V'_{max}$ (i.e. the maximum achievable absolute voltage at $Q = Q_{SC,max}$); step IV, turn the switch on to make $Q = 0$, and then turn the switch off. Therefore, the $V_{OC,max}$ and V'_{max} at low resistor was enabled by the on-state switch in steps II and IV. The simulated results in Fig. 1c shows that the CMEO state could be reached when the resistor varying from 1 Ω to 1MΩ. Correspondingly, the largest possible output energy per cycle E_m can be calculated using the following equation:

$$E_m = \frac{1}{2}Q_{sc,max}(V_{oc,max} + V'_{max}) \tag{2}$$

2.2. Transferring the maximized energy output of TENG for storage

The second part is to transfer the E_m for energy storage with as low loss as possible. Noticing TENG is a capacitive energy harvester, E_m can be regarded as the stored energy in the capacitor of TENG. For CS mode TENG, the intrinsic capacitor C_{TENG} is determined by:

$$C_{TENG} = \frac{\varepsilon_0 S}{d_0/\varepsilon + x(t)} \tag{3}$$

In which ε_0 and ε is the permittivity of vacuum and relative permittivity of dielectric layer, d_0 and S is the thickness of dielectric layer and contact area of two layer of TENG, respectively. The stored energies at $V^{=}V_{OC,max}$ and V'_{max} statuses are shown below:

$$E_s = \frac{1}{2}Q_{sc,max}V_{oc,max} \tag{4a}$$

$$E_c = \frac{1}{2}Q_{sc,max}V'_{max} \tag{4b}$$

E_S and E_C represent the stored energies in C_{TENG} at $V^{=}V_{OC,max}$ and V'_{max} statuses, respectively. If this energy is directly transferred to the stored capacitor, huge loss would occur [21,31]. Here, we employ the LC oscillating system to efficiently transfer the stored energy, which could be analyzed using the zero-input response model (The circuit diagram is illustrated in Supplementary Fig. 1 and analyzed theoretically in Supplementary Note 1). Negligible energy loss was produced in a quarter of a cycle according to the simulation results, during which the energy in C_{TENG} was transferred to the inductor (Simulated result is plotted in Supplementary Fig. 1b, and parameters for this simulation is listed in Supplementary Table 2).

The detail process can be divided into six steps as diagramed in Fig. 1d: step i, the upper part moves relatively to $x = x_{max}$ at switch off to enable $(Q,V) = (0,V_{OC}, max)$; step ii, turn the switch on to make energy stored in C_{TENG} transfer to primary inductor via LC oscillating to enable $(Q,V) = (Q_{SC},max,0)$, then turn the switch off; step iii, the upper part moves relatively from $x = x_{max}$ towards x = 0 at switch off, the stored energy in primary inductor is transferred to the capacitor for energy storage through the coupled inductor as well as the LC oscillating between the secondary inductor and the capacitor at the

same time; step iv: the upper part moves relatively to $x = 0$ at switch off to enable $(Q,V) = (Q_{SC}, max, -V'_{max})$; step v- turn the switch on to transfer the stored energy in TENG to primary inductor via LC oscillating to enable $(Q,V) = (0, 0)$; step vi, the upper part moves from $x = 0$ towards $x = x_{max}$ at switch off, meanwhile the stored energy in primary inductor is transferred to the capacitor. From the six-steps operation, we can maximize the energy obtained from TENG as well as the transfer efficiency to the capacitor.

To better understand the energy-transfer process, simulated results using SPICE software is plotted in Fig. 1e–f. After the voltage of TENG (V_T) reached its maximum value, an enable signal was applied to the switch and opened the switch, which let the stored energy in C_{TENG} transfer to the primary inductor as shown in Fig. 1e. In the enlarged figure in Fig. 1f, we could find the current of primary inductor (I_P) increased as the decrease of V_T, showing the energy transfer process lasted a quarter of a cycle (i.e. the oscillating cycle of C_{TENG} and L_P). Then the stored energy of L_P was transferred to secondary wind (L_S) of the coupled inductor as shown in Fig. 1g. We can observe the fast decrease of I_P and increase of I_S. Afterwards the stored energy of L_S transferred to capacitor via LC oscillating and increased the voltage of capacitor (V_C).

2.3. Performance of PMS for CS-mode TENG

To demonstrate the features of high-efficiency power-management and feasibility for pulse output, a CS-mode TENG is firstly used as shown in Fig. 2a. Here we employed two arch-shaped TENG using fluorocarbon plasma treated wrinkle PDMS and PET/ITO as the triboelectric layer [34–36]. The photograph of the device and SEM image of the wrinkle structure are shown in the inserted figure in Fig. 2a, each TENG has a size of 6 cm × 8 cm with a peak gap of 3 mm. Under periodical force by a vibrator, this TENG could produce a typical pulse-shaped voltage and current, while the peak value of voltage was about 374 V and the peak value of current was 15μA as plotted in Fig. 2b–c, respectively. Using the elaborated PMS for TENG, a power management module (PMM) is assembled. The key point for this PMM is the precisely control of the switch that should be turned on once the rectified voltage reached its peak value. In our work, the switch is controlled by logic circuits [31,37] that trigger by the peak value of rectified voltage (Detailed diagram for the control circuit is illustrated in Supplementary Fig. 2).

For verifying the work-well of the PMM, the output voltage and current curves of TENG was firstly measured and shown in Fig. 2d. Once the voltage reaches its peak value, a pulse current would produce along with the quickly decreasing of voltage. Enlarging these curves, an enable signal (V_S) was observed to apply to the switch and opened the switch, which let the stored energy in C_{TENG} transfer to the primary inductor as shown in Fig. 2e and cause the increase of current in primary inductor. Then the stored energy of L_P was transferred to secondary wind of the coupled inductor as shown in Fig. 2f, which afterwards transferred to the stored capacitor and increased the voltage of capacitor. The experimental results in Fig. 2e-f shown similar results with our simulations plotted in Fig. 1e-f, exhibiting the well-adaptation and efficiently energy transfer of PMM. The output voltage and current curves with 1 kΩ and 100 kΩ are measured and shown in Supplementary Fig. 3a-b, which shown the voltage curve kept almost the same while the peak current value decreased with the increasing of load resistance. Supplementary Fig. 3c presents the experimental V-Q plots with 1 kΩ and 100 kΩ load resistance, which are comparable with that shown in Fig. 1c, proving the achievement of the cycles for maximized energy output of TENG via the serial switch. Fig. 2g plotted the V-Q plot of this device using PMM, which represents the input electric energy to PMM. The $V_{OC,max}$, V'_{max}, and $Q_{sc,max}$ were 421 V, 82 V, and 202 nC, respectively, corresponding to a E_m of 93.3 μJ according to Eq. (2). The capacitor was charged to 6.65 V within 8 cycles, corresponding 221.11 μJ energy stored ($E_c = 1/2CV_C{}^2$) and
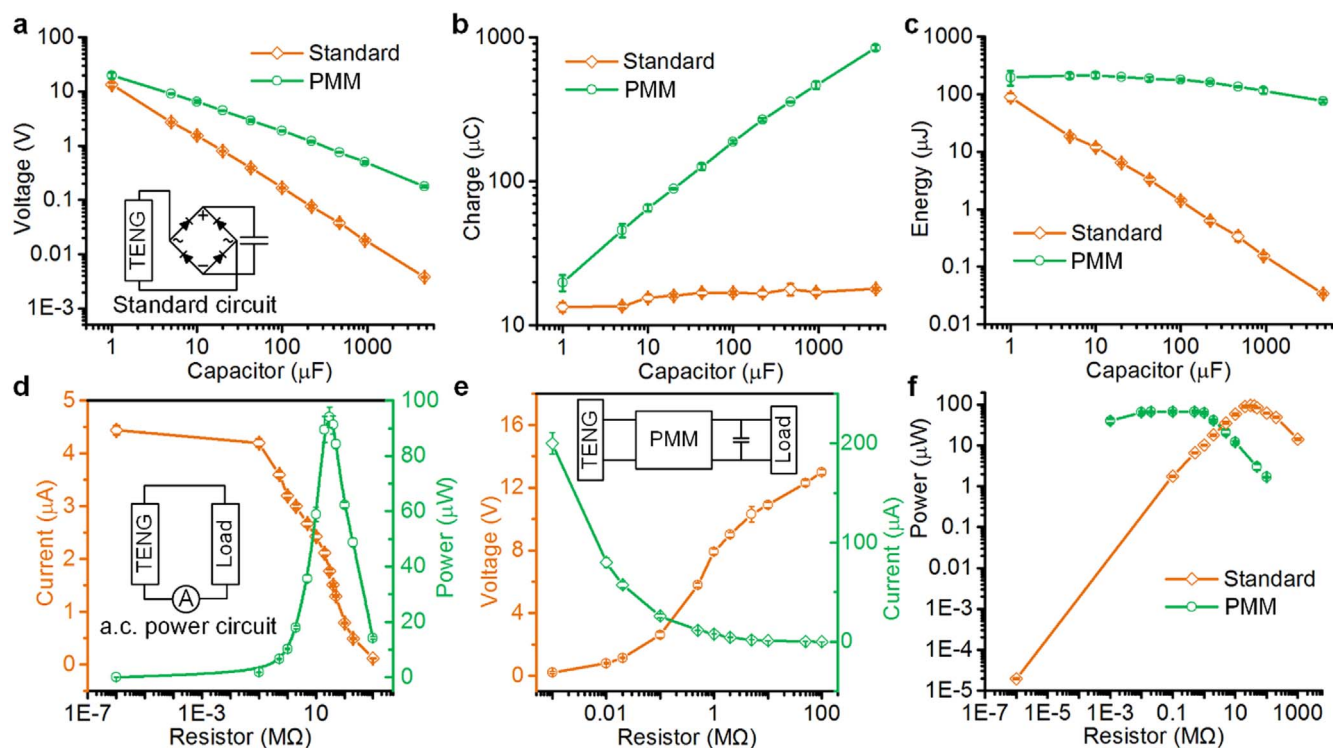
Fig. 3. Performance comparison of using PMM and standard circuit for CS-mode TENG. (**a–c**) The charging voltages, stored charges, stored energies for capacitance range from 1μF to 4.7mF of the CS-mode TENG via a standard circuit and the PMM. (**d**) The AC power curve of CS-mode TENG and its testing circuit shown in inserted figure. (**e**) The DC voltage and current of CS-mode TENG via PMM. (**f**) The experimental DC power curve via PMM and AC power curve.

27.6 μJ energy stored per cycle (E_{pc}) in this capacitor as shown in Fig. 2f. So the energy transfer efficiency η_e of PMM can be calculated to be 29.6%, this value is much better than the previous work [38].

The charging ability of the PMM was compared with a standard charging circuit for TENG using a full-wave rectifier. Charging voltages of 8 cycles for various capacitors ranging from 1 μF to 4.7 mF were shown in Fig. 3a. Both of the charging voltages from PMM and standard circuits decreased with the increase of capacitor, but the charging voltage using PMS decreased obviously much slower. When a 4.7 mF was used as the charging capacitor, 0.18 V and 0.0038 V were charged by the PMM and standard circuit, respectively (corresponding charging curves shown in supplementary Fig. 4). In this condition, the charging voltage was 47.24 times of the standard circuit. The stored charges (Q) in those capacitors (C) could be calculated by $Q = CV_C$, where V_C represents the voltage of capacitor. Fig. 3b. shows that the stored charges by standard circuit kept almost the same with the increase of capacitance, while stored charges by PMM increased from 19.8 μC to 846 μC by 4172.3% when the capacitance increased from 1 μF to 4.7 mF. Considering the stored charges by standard circuit were 17.9 μC using 4.7 mF capacitor, the stored charge by PMM increased about 46.3 times. More importantly, the stored energy ($E = 1/2CV_C^2$) by PMM kept almost the same and dropped a little from 196.02 μJ to 76.14 μJ, while the stored energy by standard circuits dropped obviously from 89.78 μJ to 0.034 μJ when the capacitance increase from 1μF to 4.7 mF as plotted in Fig. 3c. In practice, a large capacitor was usually used to store the electric energy generated by TENG, which make it very important to transfer as much as possible energy to the large capacitor. When using a 4.7 mF, the stored energy by PMM was 2640 times higher than the standard circuit!.

For a continuously working TENG, it's of significant importance to obtain the maximum output power (P) by varying the outer load, which is one of the most used parameters for evaluating TENG's performance. As a power management system, one of the most important parameter for the PMM is the total power efficiency η_{total}, which is defined as the ratio of the maximum DC power stored in the storage unit to the

maximum alternating current (AC) power delivered to a resistive load [31]. To measure η_{total}, we firstly measured the maximum AC power delivered to a resistive load extracted by measuring the Root-Mean-Square (RMS) value of current using resistors with different values and then calculating the effective power by equation $P = I^2R$. As shown in Fig. 3d, the maximum AC power generated by TENG was 93.99 μW at an optimum load resistance of 30 MΩ. The DC power stored in the storage unit is obtained by measuring the DC voltage of a varying parallel resistor as shown in Fig. 3e. Afterwards the DC power was calculated by the equation $P = V^2/R$, and a maximum DC power of 67.6 μW was reached at an equivalent resistance of 100 KΩ (Fig. 3f.). Therefore, the total efficiency of PMS for this TENG was calculated to be 71.9%. Considering the consumption of logic circuits, this efficiency still kept at very high level of 69.1%, which is the highest record to the best of our knowledge for the CS-mode TENG (The power consumption for the logic circuits is calculated in Supplementary Note 3). Besides, the optimal resistance of TENG was significantly decreased from 30 MΩ to 100 KΩ, while the range of the optimal resistance was obviously broadened (i.e. the DC power kept over 62 μW in the resistance range from 10 KΩ to 1 MΩ).

2.4. Performance of PMM for LS-mode TENG

To further validate the universality of the PMM for different kinds of output waveforms, the performance of PMM for LS-mode TENG was measured as follows. The single unit and 3D diagram for the LS-mode TENG we used in this work were shown in Fig. 4a. The traditional free-standing mode TENG was employed to produce output signal with uniform triangular shape. Different from the CS-mode TENG, the lateral direction was defined as the movement direction (i.e. x). Under the mechanical motions driven by a person's hand, the LS-mode TENG could produce a uniform and triangular waveform with a peak voltage of 225 V and maximum current of 18 μA as shown in Fig. 4b-c. To provide stable and comparable results, the sliding frequency was kept at 0.5 Hz. In comparing with a standard circuit, all the results are an average value of 7
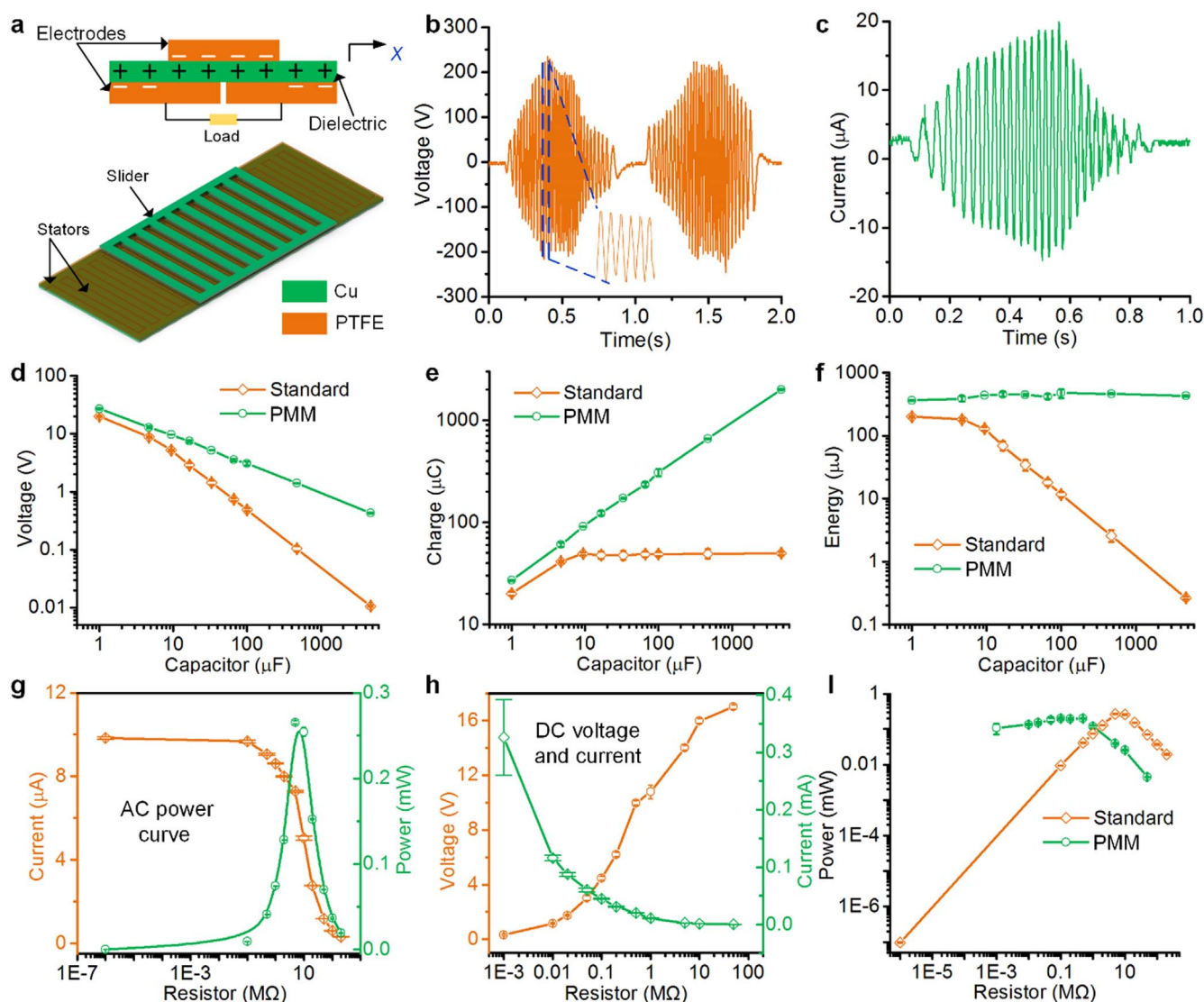
Fig. 4. Experimental results using PMM for LS-mode TENG. (**a**) Schematic diagram and definition of sliding direction x of the LS-mode TENG using in this work. (**b–c**) Waveforms of output voltage and current of the LS-mode TENG. (**d–f**) The charging voltages, stored charges, stored energies for capacitance range from 1μF to 4.7mF of the LS-mode TENG via a standard circuit and the PMM. (**g**) The AC power curve of LS-mode TENG. (**h**) The DC voltage and current of LS-mode TENG via PMM. (**i**) The experimental DC power curve via PMM and AC power curve of LS-mode TENG.

semi-cycles (i.e. one direction slides from one side to the other side). When using the LS-mode TENG as power source, the PMM shown similar and even better results compared with CS-mode TENG: the charging voltage using PMM had a much slower decreasing speed as the increase of the capacitance, and the charging voltage (0.427 V) using PMS was 40.28 times at 4.7 mF capacitance of the standard circuit (0.0106 V) as plotted in Fig. 3d; The transferred charges with standard circuit saturated at 49.82 μC, while the transferred charges using PMS increased along to 2.01 mC, which was improved by 40.35 times (Fig. 4d); though the stored energy by standard circuit decreased dramatically from 200.5 μJ to 0.26 μJ during the capacitance interval from 1 μF to 4.7 mF, the stored energy using PMM kept almost the same and even had a value of 428.5 μJ at 4.7 mF as shown in Fig. 4f, which was improved by 1648.1 times at 4.7 mF!.

The following experiments were carried out to obtain the total efficiency of PMM for LS-mode TENG. As shown in Fig. 4g, the maximum AC power generated by LS-mode TENG was 0.265 mW at an optimum load resistance of 5 MΩ. The DC power stored in the storage unit was obtained by measuring the DC voltage of a varying parallel resistor as shown in Fig. 4h. A maximum DC power of 0.2 mW was reached at an equivalent resistance of 100 KΩ (Fig. 4i). Therefore, the total efficiency of PMM for this LS-mode TENG was calculated to be

75.5%. Considering the consumption of logic circuits, this efficiency was 74.45% (The power consumption for the logic circuits is calculated in Supplementary Note 3). Meanwhile, the DC power curve was also broadened than the AC power curve, which made it easier to match the optimal resistance for maximum power output.

2.5. Boosting the drive capability of TENG for electronics

Due to extraordinary performance of the PMM for boosting the charging ability for energy storage unit and high efficiency in DC power conversion, this module could be employed to effectively and efficiently manage the AC power to supply power for traditional electronics. As an example, an energy flow chart for scavenging mechanical energy to power electronics is diagramed in Fig. 5a. TENG was employed to extracted the mechanical energy from a person to electric energy. Then it was managed by PMM to be converted to DC power, and afterwards stored in a battery or a capacitor. Finally, we can use the stored electric energy to power electronic tools with various function (e.g. a calculator) and wearable electronics to monitor the human motion in real-time, forming a totally self-powered system. Fig. 5b shows the circuit diagram of PMM with a capacitor as the energy storage unit. Trigged by a person's hand, the CS-
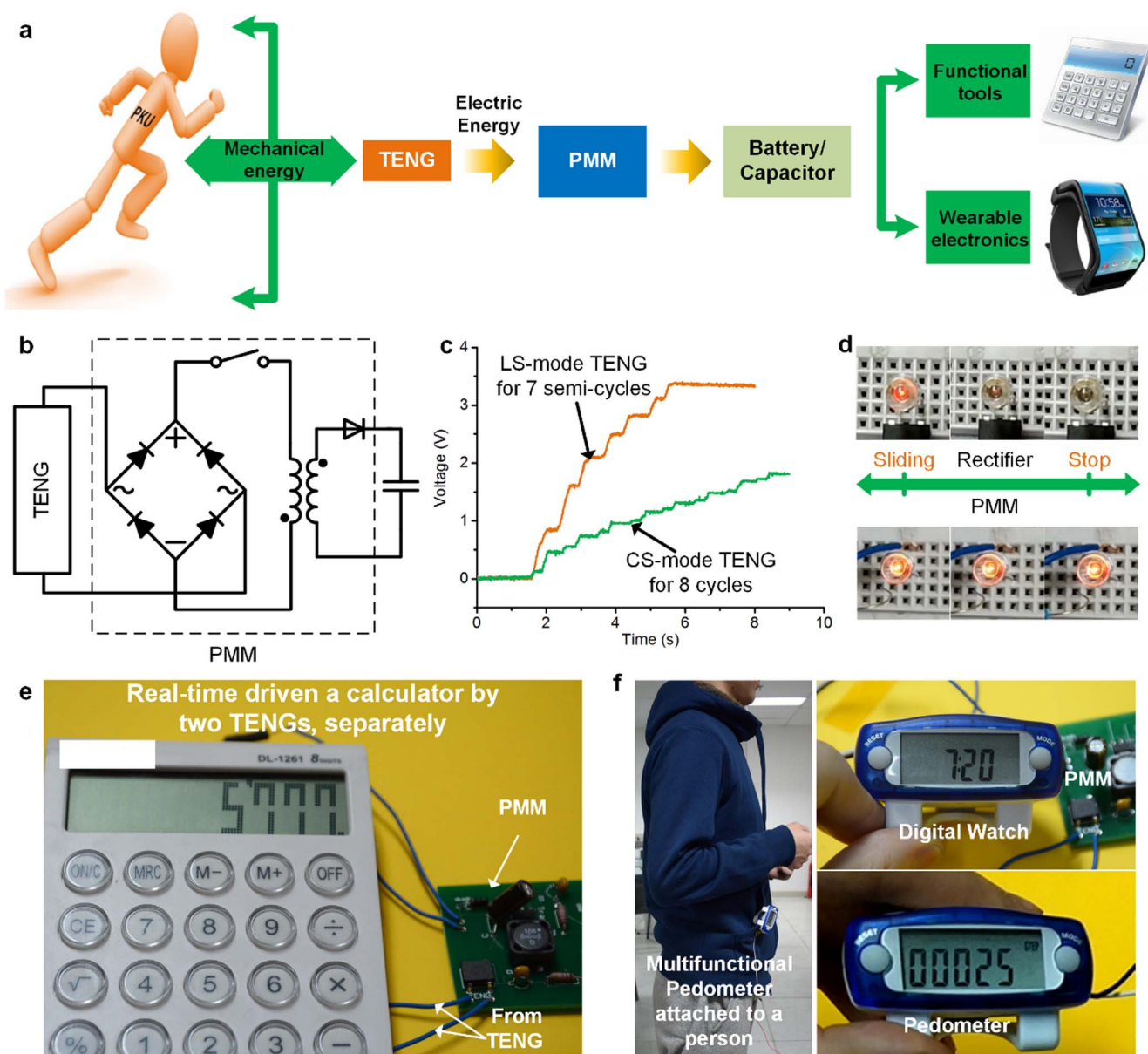
Fig. 5. Demonstrations of using managed DC energy for powering electronics. (**a**) TENG based energy flow chart for scavenging mechanical energy to power electronics. (**b**) The circuit diagram of PMM. (**c**) Charging curves of LS-mode TENG and CS-mode TENG via PMM for a 47 µF commercial capacitor. (**d**) Comparison of using LS-mode TENG to power a red LED via a commercial rectifier and PMM. (**e**) Real-time driven a normally working calculator by two modes TENGs via PMM, separately. (**f**) Suppling power for a multifunctional pedometer.

mode TENG could charge a 47 µF TENG to 1.82 V within 8 cycles, while the LS-mode TENG could charge this capacitor to 3.45 V within 7 semi-cycles as plotted in Fig. 5c. When directly powering a red LED bulb via a rectifier using both modes TENGs respectively, the LED bulb would be illuminated instantaneously as shown in Fig. 5d and Supplementary Video 1 and 2. But using the PMM to power this LED, it would be continuously turned on with enhanced brightness. Using the stored DC power, a commercial calculator could be successfully driven in a real-time way and normally calculate at a very low working frequency of TENGs (< 2 Hz), while both modes TENG used in this work exhibited similar results. (Supplementary Video 3–4). For powering wearable electronics, a commercial multifunction pedometer attached to a person was powered by the LS-mode TENG using PMM, as shown in Fig. 5f and the Supplementary Video 5. With the PMM, this multifunctional device could work continuously to display time, walking steps as well as the consumed calories.

Supplementary material related to this article can be found online at http://dx.doi.org/10.1016/j.nanoen.2017.05.063.

3. Discussion

We have developed a universal and efficiently power management strategy for TENGs through theoretical deviation, simulation analysis, experimental validation and practical demonstration. Employing the built-up voltage V-transferred charge Q plot, the CMEO with low resistance and a serial switch was derived to have the maximized output energy per cycle, which is the maximum energy production of a given TENG. Using the LC oscillating to transfer the maximized energy to the storage unit, realizing high efficiency energy transfer. Then the PMM using this strategy was successfully utilized to manage the pulse output from a CS-mode TENG as well as a uniform triangular output from a LS-mode TENG. Different from the feature of constant transferred charge using traditional circuits, the PMM exhibited the highly-appreciated advantage in constant energy transfer for various capacitance, resulting in 2640 times of standard circuit energy storage in a 4.7 mF capacitor. High AC to DC power conversion efficiency was

observed both for the CS-mode TENG and the LS-mode TENG with total efficiency of 71.9% and 75.5%, which are the highest reported to the best of our knowledge. Due to this, the managed DC power was able to continuously power commercial electronics. Including LED bulb, calculator, multifunctional pedometer can successfully work in real-time with a very low working frequency of TENG (< 2 Hz). This work provides a universal power management strategy for TENG both in theoretical and simulation ways, which could undoubtedly improve the practical value of TENG and may speed up its industrialization process.

4. Methods

4.1. Fabrication of the CS-mode TENG

It starts with an indium tin oxide (ITO) coated polyethylene ter-ephthalate (PET) fi lm. The vacuum degassed PDMS mixture is then spin coated on it. A C_4F_8 plasma treatment process is carried out in an inductively coupled plasma etching machine before PDMS is cured. The wrinkle structure would be formed in this process. After the PDMS is cured, the processed PDMS film is assembled with another PET/ITO film to form an arch-shape TENG. Finally, two arch-shaped TENGs were attached together as the CS-mode TENG used in this work.

4.2. Fabrication of the LS-mode TENG

The fabrication of the electrode networks of stator and slider is a well-known high-throughput flexible printing electronics technology. The fabrication procedure starts from two sheets of commercial flexible copper clad laminate (FCCL). The FCCL consists of a flexible polyimide substrate and one copper films with thin layers of epoxy adhesive in between. The copper films were patterned by photolithography and etched by $FeCl_3$ solution to fabricate the interdigital electrode on stator and complementary grid on the slider. Finally, a layer of polytetra-fluoroethylene (PTFE) as an electrification material with a thickness of 50 μm was laminated on the electrode of slider.

4.3. Simulation methods

The simulation process included electrostatic simulation and load-circuit simulation. For electrostatic simulation, the COMSOL electro-static module was utilized to calculate $V_{OC}(x)$ and $C(x)$. Then, from continuous fraction interpolation, a numerical $V_{OC}(x)$ and $C(x)$ relationship could be generated in the entire x region. Afterwards, we embedded the above TENG model into the SPICE software as an element consisting of a voltage source ($V_{OC}(x)$) in serial connection with a capacitor($C(x)$). So we can add switch, inductor, capacitor and resistor mentioned in this work to simulate the electric output such as open circuit voltage, short-circuit current, and we can get all the simulation results used in this work.

4.4. Electrical measurements

The output voltage of TENG was measured via a digital oscilloscope (Agilent DSO-X 2014A) using a 100 MΩ probe (HP9258), and the current was amplified by a SR570 low noise current amplifier from Stanford Research systems. Open circuit voltage of TENG was measured using the Keithley 6514 System Electrometers.

Competing financial interests

The authors declare no competing financial interests.

Acknowledgements

Appendix A. Supporting information

Supplementary data associated with this article can be found in the online version at doi:10.1016/j.nanoen.2017.05.063.

References

[1] J.A. Rogers, T. Someya, Y. Huang, Materials and mechanics for stretchable electronics, Science 327 (2010) 1603–1607.
[2] J.P. Lynch, K.J. Loh, A summary review of wireless sensors and sensor networks for structural health monitoring, Shock Vib. Dig. 38 (2006) 91–130.
[3] D.H. Kim, D.L. Kaplan, et al., Dissolvable films of silk fibroin for ultrathin conformal bio-integrated electronics, Nat. Mater. 9 (2010) 511–517.
[4] H. Wu, Y. Cui, Designing nanostructured Si anodes for high energy lithium ion batteries, Nano Today 7 (2012) 414–429.
[5] J.B. Goodenough, K.S. Park, The Li-ion rechargeable battery: a perspective, J. Am. Chem. Soc. 135 (2013) 1167–1176.
[6] C. Liu, Z. Yu, D. Neff, A. Zhamu, B.Z. Jang, Graphene-based supercapacitor with an ultrahigh energy density, Nano Lett. 10 (2010) 4863–4868.
[7] S.P. Beeby, M.J. Tudor, N.M. White, Energy harvesting vibration sources for microsystems applications, Meas. Sci. Technol. 17 (2006) R175.
[8] P.D. Mitcheson, E.M. Yeatman, G.K. Rao, A.S. Holmes, T.C. Green, Energy harvesting from human and machine motion for wireless electronic devices, Proc. IEEE 96 (2008) 1457–1486.
[9] A. Costanzo, M. Dionigi, D. Masotti, M. Mongiardo, G. Monti, L. Tarricone, R. Sorrentino, Electromagnetic energy harvesting and wireless power transmission: a unified approach, Proc. IEEE 102 (2014) 1692–1711.
[10] Y. Suzuki, D. Miki, M. Edamoto, M. Honzumi, A MEMS electret generator with electrostatic levitation for vibration-driven energy-harvesting applications, J. Micromech. Microeng. 20 (2010) 104002.
[11] Z.L. Wang, J. Song, Piezoelectric nanogenerators based on zinc oxide nanowire arrays, Science 312 (2006) 242–246.
[12] F.R. Fan, Z.Q. Tian, Z.L. Wang, Flexible triboelectric generator, Nano Energy 1 (2012) 328–334.
[13] Z.L. Wang, Triboelectric nanogenerators as new energy technology for self-powered systems and as active mechanical and chemical sensors, ACS Nano 7 (2013) 9533–9557.
[14] X.S. Zhang, M. Su, J. Brugger, et al., Penciling a triboelectric nanogenerator on paper for autonomous power MEMS applications, Nano Energy 33 (2017) 393–401.
[15] X. Cheng, Y. Song, H. Zhang, et al., A flexible large-area triboelectric generator by low-cost roll-to-roll process for location-based monitoring, Sens. Actuators A: Phys. 247 (2016) 206–214.
[16] X.S. Zhang, J. Brugger, B. Kim, A silk-fibroin-based transparent triboelectric generator suitable forautonomous sensor network, Nano Energy 20 (2016) 37–47.
[17] J. Chen, J. Yang, Z. Li, X. Fan, Y. Zi, Q. Jing, Z.L. Wang, Networks of triboelectric nanogenerators for harvesting water wave energy: a potential approach toward blue energy, ACS Nano 9 (2015) 3324–3331.
[18] J. Bae, J. Lee, S. Kim, J. Ha, B.S. Lee, Y. Park, J.J. Park, Flutter-driven triboelectrification for harvesting wind energy, Nat. Commun. 5 (2014).
[19] X. Cheng, B. Meng, X. Zhang, M. Han, Z. Su, H. Zhang, Wearable electrode-free triboelectric generator for harvesting biomechanical energy, Nano Energy 12 (2015) 19–25.
[20] Q. Zheng, B. Shi, F. Fan, X. Wang, L. Yan, W. Yuan, Z.L. Wang, In vivo powering of pacemaker by breathing-driven implanted triboelectric nanogenerator, Adv. Mater. 26 (2014) 5851–5856.
[21] S. Niu, Z.L. Wang, Theoretical systems of triboelectric nanogenerators, Nano Energy 14 (2015) 161–192.
[22] Y. Song, X. Cheng, H. Chen, J. Huang, X. Chen, M. Han, H. Zhang, Integrated self-charging power unit with flexible supercapacitor and triboelectric nanogenerator, J. Mater. Chem. A 4 (2016) 14298–14306.
[23] S. Wang, L. Lin, Z.L. Wang, Nanoscale triboelectric-effect-enabled energy conver-sion for sustainably powering portable electronics, Nano Lett. 12 (2012) 6339–6346.
[24] Y. Yang, H. Zhang, Z.H. Lin, Y.S. Zhou, Q. Jing, Y. Su, Z.L. Wang, Human skin based triboelectric nanogenerators for harvesting biomechanical energy and as self-powered active tactile sensor system, ACS Nano 7 (10) (2013) 9213–9222.
[25] S. Wang, L. Lin, Y. Xie, Q. Jing, S. Niu, Z.L. Wang, Sliding-triboelectric nanogenerators based on in-plane charge-separation mechanism, Nano Lett. 13 (2013) 2226–2233.
[26] S. Wang, Y. Xie, S. Niu, L. Lin, Z.L. Wang, Freestanding triboelectric-layer-based nanogenerators for harvesting energy from a moving object or human motion in contact and non-contact modes, Adv. Mater. 26 (18) (2014) 2818–2824.
[27] Z.L. Wang, J. Chen, L. Lin, Progress in triboelectric nanogenerators as a new energy technology and self-powered sensors, Energy Environ. Sci. 8 (2015) 2250–2282.
[28] C. Han, C. Zhang, W. Tang, X. Li, Z.L. Wang, High power triboelectric nanogen-erator based on printed circuit board (PCB) technology, Nano Res. 8 (3) (2015) 722–730.

[29] X. Pu, M. Liu, L. Li, C. Zhang, Y. Pang, C. Jiang, Z.L. Wang, Efficient charging of li-ion batteries with pulsed output current of triboelectric nanogenerators, Adv. Sci. 3 (2016).

[30] Y. Zi, H. Guo, Z. Wen, M.H. Yeh, C. Hu, Z.L. Wang, Harvesting low-frequency (< 5 Hz) irregular mechanical energy: a possible killer application of triboelectric nanogenerator, ACS Nano 10 (2016) 4797–4805.

[31] S. Niu, X. Wang, F. Yi, Y.S. Zhou, Z.L. Wang, A universal self-charging system driven by random biomechanical energy for sustainable operation of mobile electronics, Nat. Commun. 6 (2015).

[32] Y. Zi, S. Niu, J. Wang, Z. Wen, W. Tang, Z.L. Wang, Standards and figure-of-merits for quantifying the performance of triboelectric nanogenerators, Nat. Commun. 6 (2015).

[33] G. Cheng, Z.H. Lin, L. Lin, Z.L. Du, Z.L. Wang, Pulsed nanogenerator with huge instantaneous output power density, ACS Nano 7 (8) (2013) 7383–7391.

[34] X. Cheng, B. Meng, X. Chen, et al., Single-step fluorocarbon plasma treatment-induced wrinkle structure for high-performance triboelectric nanogenerator, Small 12 (2016) 229–236.

[35] X. Cheng, X. Chen, B. Meng, et al. A flexible and wearable generator with fluorocarbon plasma induced wrinkle structure. 2016 IEEE in: Proceedings of the 29th International Conference on Micro Electro Mechanical Systems (MEMS). IEEE, Q7 1181–1184, 2016.

[36] X. Cheng, L. Miao, Z. Su, et al., Controlled fabrication of nanoscale wrinkle structure by fluorocarbon plasma for highly transparent triboelectric nanogenerator, Microsyst. Nanoeng. 3 (2017) 16074.

[37] S. Boisseau, G. Despesse, S. Monfray, O. Puscasu, T. Skotnicki, Semi-flexible bimetal-based thermal energy harvesters, Smart Mater. Struct. 22 (2013) 025021.

[38] Y. Zi, H. Guo, J. Wang, Z. Wen, S. Li, C. Hu, Z.L. Wang, An inductor-free auto-power-management design built-in triboelectric nanogenerators, Nano Energy 31 (2017) 302–310.

Zong-Ming Su received the B.S. degree from the University of Science and Technology Beijing, in 2013. He is currently pursuing the Ph.D. degree at the National Key Laboratory of Nano/Micro Fabrica-tion Technology, Peking University, Beijing, China. His research interests are micro & Nano structure fabrication and energy harvesting.

Hao-Tian Chen received the B. S. degree from Dalian University of Technology, China, in 2013. He is currently pursuing the Ph.D. degree at the National Key Laboratory of Nano/Micro Fabrication Technology, Peking University, Beijing, China. His research mainly focuses on energy harvesters and electronic skins.
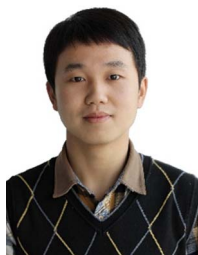

Xiao-Liang Cheng received the B.S. degree from the University of Electronic Science and Technology of China, Chengdu, in 2014. He is currently pursuing the Ph.D. degree at the National Key Laboratory of Nano/Micro Fabrication Technology, Peking University, Beijing, China. His research interests mainly include design and fabrication of nanogenerator and mechanical energy harvester.

Xue-Xian Chen received the B.S. degree from the University of Electronic Science and Technology of China, Chengdu, in 2015. She is currently pursuing the Ph.D. degree at the National Key Laboratory of Nano/Micro Fabrication Technology, Peking University, Beijing, China. Her research interests mainly include design and fabrication of hybrid nanogenerator and electrospinning process.

Li-ming Miao received the B.S. degree from Peking University, Beijing, in 2017. His research interests mainly include wrinkle structure and triboelectric nanogenerator.

Jin-Xin Zhang received the B.S. degree from the School of Electronics Engineering and Computer Science, Peking Uni-versity, Beijng, in 2016. He is currently pursuing the Ph.D. degree at the National Key Laboratory of Nano/Micro Fabrication Technology, Peking University, Beijing, China. His re-search interests mainly include electronic skin design and pressure sensor fabrication.

Yu Song received the B.S. degree in Electronic Science & Technology from Huazhong University of Science and Tech-nology, China, in 2015. He is currently pursuing the Ph.D. de-gree at the National Key Laboratory of Nano/Micro Fabrica-tion Technology, Peking University, Beijing, China. He majors in MEMS and his research is focusing on supercapacitors and self-charging power system.

Hai-Xia (Alice) Zhang received the Ph.D. degree in mechanical engineering from Huazhong University of Science and Technology, Wuhan, China, 1998. She is cur-rently a Professor with the Institute of Microelectronics, Peking University, Beijing, China. She joined the faculty of the Institute of Microelectronics in 2001 after finishing her post-doctoral research in Tsinghua University. Her research interests include MEMS design and fabrication technology, SiC MEMS, and micro energy technology.